Microwave Review
July 2025, Vol. 31, No. 1, pp. 39-43
DOI: 10.18485/mtts_mr.2025.31.1.7

Ultrashort Pulse Decomposition in a Two-Turn Meander Line with Radio Absorbing Material

Georgiy Y. Kim, Alexander V. Nosov

Abstract – **This paper presents practical realization of a two-turn meander microstrip line with reduced size. For the first time, two approaches were applied for this purpose: the use of radio absorbing material (RAM) and additional folding of each meander line turn into non-core turns. It was revealed that the sequences of arrival of decomposed pulses in structures with and without RAM differ. In this regard, new conditions for decomposition of ultrashort pulse (USP) were formulated. It was revealed that folding of each turn of meander microstrip line into minor turns leads to additional attenuation of the USP. According to the experimental results, the attenuation of a USP in such a structure was 15.3 dB. The width and length of the fabricated prototype were 46 mm and 57 mm. By contrast, without using RAM and folding, the dimensions were 10 mm and 575 mm, and the attenuation of a USP was only 4.08 dB. The analysis of the *N*-norms of the studied structure showed, that *N*1, *N*2, *N*3, and *N*5 decreased by 5.75 times, 13.16 times, 1.04 times, and 2.92 times, while *N*4 increased by 1.54 times. The structure can be used in DC power circuits with voltages and currents up to 530 V and 850 mA.**

Keywords – **Ultrashort pulse, Protective device, Meander line, Radio absorbing material**

I. Introduction

With the development of electronic devices, the operating voltages are decreasing and the density of printed circuit board (PCB) traces is increasing. These technological changes increase the susceptibility of electronic devices to various types of electromagnetic interference (EMI). It is known that EMI can be a threat to modern electronic devices [1, 2]. Thus, generators of powerful EMI can be used by intruders to destabilize or completely disable critical infrastructure [3–6]. Ultrashort pulses (USPs) are a serious threat to electronic devices [7]. There are many well-known traditional techniques to protect devices against USPs, but they have several disadvantages, namely low power and speed, as well as limited resource [8]. Therefore, it is relevant to search for new approaches and protective devices that do not have these disadvantages. Engineers have developed multiple devices based on printed structures for protection against EMI and signal filtering in the frequency band [9–11]. One of the promising approaches to protect electronic equipment is the one based on the USP attenuation in the meander line (ML) due to modal decomposition [12]. It seems promising because the implementation of such protection may not require an additional protective device but can utilize the MLs already available on the PCB. The principle of this approach is to decompose the USP into a sequence of crosstalk pulses, odd and even modes of smaller amplitudes in a meander microstrip line (MSL), and then equalize their amplitudes. This allows attenuating the USP amplitude by 7.6 dB in the simplest case [12]. However, such attenuation is not sufficient to protect electronic equipment from powerful USPs. To solve this problem, a meander MSL of several turns connected in series can be used. In such structures, the USP is first decomposed into a sequence of pulses of smaller amplitudes in the first turn, and then each of them - in the turn that follows, etc. Thus, the use of a meander MSL of 2 turns allowed increasing the attenuation up to 14.3 dB, of 3 turns up to 18.2 dB, of 4 turns up to 26 dB, and of 5 turns up to 30.4 dB [13, 14]. However, practical realization and further use of such structures in modern electronic equipment is very difficult. This is explained by the need to use lines with high length and/or substrates with large dielectric constant. To solve the problems described above, the following approaches can be used: the use of radio absorbing material (RAM) and additional folding of each ML turn into non-core turns. The first approach allows achieving a large difference in the decomposition mode delays ($\Delta\tau$) using available dielectric substrates [15], while the second approach reduces the size of the final protective device and additionally weakens the USP due to the presence of oscillations at its output [16]. Note that in the presence of RAM in the structure, the arrival sequence of decomposition pulses at its output will change compared to previous results from [13, 14]. This will require the formulation of new conditions for the decomposition of the USP for use in optimization. However, the use of these approaches for structures of two or more turns has not been previously considered. That's why it's relevant. It is advisable to improve a simpler structure due to RAM and folding of turns: a meander MSL of two turns. Thus, the goal of this work is to improve the meander MSL with two turns by folding and covering it with RAM.

Article history: Received November 25, 2024; Accepted April 18, 2025

Georgiy Y. Kim and Alexander V. Nosov are with the research laboratories «Fundamental Research in Electromagnetic Compatibility» and «Safety and electromagnetic compatibility of radio-electronic means», Vershinina 47, 634045 Tomsk, Russia, E-mail: kimgeoju@gmail.com, alexns2094@gmail.com

II. Initial Data

This study investigates a two-turn meander MSL connected in series. In such a structure, when the cross-section parameters are optimal, the USP is initially decomposed into three pulses in the first turn, and then each of them is decomposed into three more pulses in the second turn. The connection diagram of the structure is shown in Fig. 1.

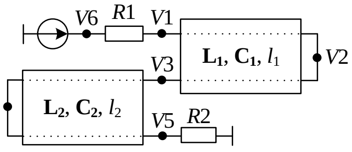

Fig. 1. Circuit diagram of a two-turns meander MSL

Resistors $R1$ and $R2$ are assumed to be 50 Ω each. The cross-section, which is the same for each turn, is shown in Fig. 2.

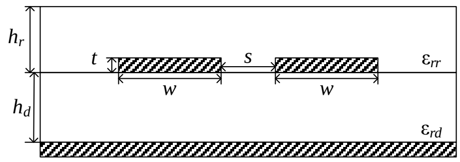

Fig. 2. Cross-section, which is the same for each turn

For further simulation, excitation is assumed to be a USP with 1 V e.m.f. and duration of fronts and flat top of 0.2 ns each. Its voltage waveform is presented in Fig. 3.

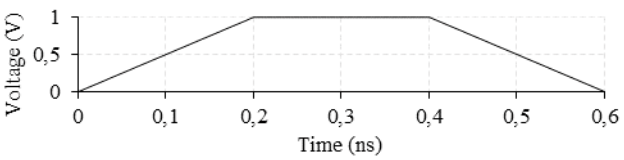

Fig. 3. Excitation signal waveform

To simplify further manufacturing and mounting of SMA connectors, the width of the conductors was chosen to be w=1 mm. The thickness of the metallized layer and the substrate were chosen from standard values provided by PCB manufacturers, i.e., t=35 μm and h_d=2 mm. FR-4 material with ε_{rd}=4.6 and $tg\delta$=0.017 was chosen for the PCB substrate. In order to obtain a large $\Delta\tau$, we chose the microwave energy absorber ZIPSIL 410 RPM-L with ε_{rr}=20.1 and $tg\delta$=0.06 as the top layer. Its thickness was set to h_r=1000 μm to ensure the maximum $\Delta\tau$ according to [15]. A heuristic optimization of the parameter s was performed using the criterion of matching the structure with the 50 Ω path. As a result, was found s=335 μm, at which $(Z_eZ_o)^{0.5}$ of each turn is equal to 49.8 Ω. These parameters will be referred to as the initial parameters, and the structure in Fig. 1 as Structure 1.

III. Simulation Results

Matrices **C** and **L** calculated in the TALGAT system [17] were the same for each turn of Structure 1:

$$\mathbf{C}=\begin{bmatrix}0.25 & -0.17\\ -0.17 & 0.25\end{bmatrix}\text{nF/m}, \mathbf{L}=\begin{bmatrix}0.52 & 0.25\\ 0.25 & 0.52\end{bmatrix}\mu\text{Hn/m}.$$

Calculated per-unit-length delays of even and odd modes were the same for each turn: τ_e=8.01 ns/m and τ_o=10.61 ns/m. It is worth noting that in the absence of a covering layer in Structure 1, $\tau_o<\tau_e$, but its $\Delta\tau$ is small, so it is necessary to use a dielectric substrate with a large ε_{rr} or a large length of its segments. As mentioned above, the sequence of pulse arrivals in Structure 1 will change compared to the results of [13]. Taking this into account, new conditions for the complete decomposition of USP in such a structure were formulated:

$$2l_1\tau_{e1} \ge t_\Sigma \quad (1)$$

$$2l_1\tau_{o1} \ge 2l_1\tau_{e1} + t_\Sigma \quad (2)$$

$$2l_2\tau_{e2} \ge 2l_1\tau_{o1} + t_\Sigma \quad (3)$$

$$2l_2\tau_{o2} \ge 2l_2\tau_{e2} + t_\Sigma \quad (4)$$

$$2l_2\tau_{e2} + 2l_1\tau_{e1} \ge 2l_2\tau_{o2} + t_\Sigma \quad (5)$$

$$2l_2\tau_{o2} + 2l_1\tau_{e1} \ge 2l_2\tau_{e2} + 2l_1\tau_{o1} + t_\Sigma \quad (6)$$

where $\tau_{e1,2}$ and $\tau_{o1,2}$ are the per-unit-length delays of the even and odd modes of the first and second turns, and l_1 and l_2 are the lengths of their half-turns.

The lengths of the turns for which the conditions (1)–(6) are almost fulfilled were found: l_1=150 mm and l_2=250 mm. The delays of the main decomposition pulses at the output of the considered structure were calculated using the formula from [18] and are as follows: $P1$=0 ns, $P2$=2.4 ns, $P3$=3.2 ns, $P4$=4 ns, $P5$=5.3 ns, $P6$=6.4 ns, $P7$=7.2 ns, $P8$=7.7 ns, and $P9$=8.5 ns. In this case, each of the pulses will not arrive earlier than the previous ones, except for $P8$ because condition (6) is fulfilled incompletely. However, taking into account the USP duration, it will overlap insignificantly with the decay of $P7$ and will not lead to a significant increase in the resulting amplitude. This overlap can be seen in more detail from the voltage waveform in Fig. 4. In this respect, it makes no sense to increase l_2 or decrease l_1 in order to fully satisfy conditions (1)–(6).

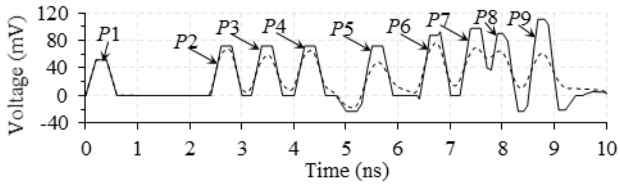

Fig. 4. Voltage waveforms at the output of Structure 1 with (– –) and without (—) losses

Figure 4 shows the voltage waveforms at the output of Structure 1 calculated using the TALGAT system. These waveforms were calculated without and with losses in conductors and dielectric and illustrate the decomposition of a USP into nine pulses. It is clear that the USP in Structure 1 is decomposed into nine basic pulses as in the MSL without RAM [18]. In this case, $P1$ is crosstalk at node $V5$ (P_{x2}) from the crosstalk pulse induced from node $V1$ to node $V3$ (P_{x1}) and then to node $V5$. $P2$ is P_{x2} from the even mode of the first turn (P_{e1}), $P3$ is P_{x2} of the odd mode of the first turn (P_{o1}), $P4$ is the even mode of the second turn (P_{e2}) of P_{x1}, $P5$ is the odd mode of the second turn (P_{o2}) of P_{x1}, $P6$ is P_{e2} of P_{e1}, $P7$ is P_{e2} of P_{o1}, $P8$ is P_{o2} of P_{e1}, and $P9$ is P_{o2} of P_{o1}. The delays of the main pulses correspond to those calculated above. It can also be seen that the rise of $P8$ is superimposed on the fall of $P7$, but this does not lead to an increase in the resulting amplitude. This happened because condition (6) was fulfilled incompletely. The maximum attenuation of USP (relative to $E/2$) at the output of Structure 1 with losses was 16.3 dB, and without losses it was 13.1 dB.

Figure 5 shows the voltage waveform at the output of a one-turn meander MSL with the initial parameters for comparison.

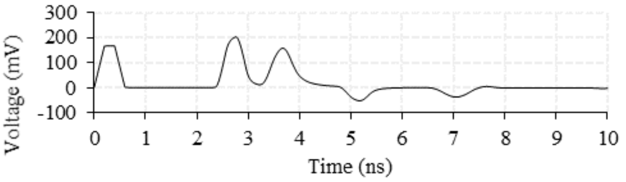

Fig. 5. Voltage waveforms at the output one ML turn with losses

It is clear that the USP is decomposed into three pulses, and its attenuation was 7.9 dB (less than in structure 1 by more than 2 times).

In order to reduce the size of the final device, we folded each turn into non-main turns, also similar to [16]. This approach allows reducing the length of the structure by increasing its width. In addition, depending on the distance between the non-core turns, oscillations appear at the output of the structure, which can further increase the USP attenuation. The optimization of the structure was carried out heuristically based on the dimensional criterion. As a result, each line in Fig. 1 was folded into five non-core half-turns. The connection diagram of such a structure is shown in Fig. 6 (for simplicity, this structure will be referred to as Structure 2), where s is the distance between the main pair of folded conductors and equals 335 µm, and s_{nv} is the distance between the non-core half-turns.

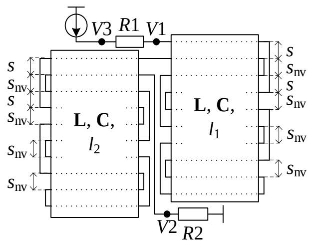

Fig. 6. Circuit diagram of the Structure 2

The value of s_{nv} was chosen according to the simulation results. The lengths of such folded turns were l_1=30 mm and l_2=50 mm.

Figure 7 shows the voltage waveforms at the output of Structure 1 and Structure 2 at s_{nv}=2200 µm, 7700 µm, and 13200 µm to demonstrate the effect of oscillations on the voltage waveforms as the coupling between non-core half-turns increases.

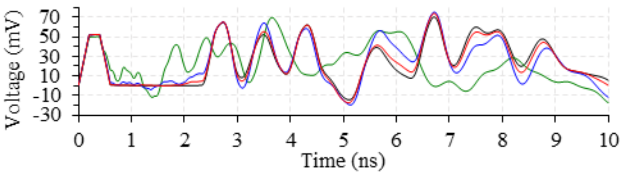

Fig. 7. Voltage waveforms at the output of Structure 1 (—) and Structure 2 with s_{nv}=2200 µm(—), 7700 µm(—), and 13200 µm(—)

It is clear that as the s_{nv} of Structure 2 increases, the quantitative and qualitative agreement with the voltage waveform at the output of Structure 1 improves. As the s_{nv} decreases, the voltage waveform is distorted, but the voltage amplitude decreases. This can be caused by the superposition of oscillations of different polarity resulting from coupling between non-core half-turns, also similar to [16]. Table 1 summarizes the maximum amplitudes (V_{max}) and USP attenuation values (E_{att}) at the output of Structure 2 at s_{nv}=2200 µm, 7700 µm, and 13200 µm.

TABLE 1
THE MAXIMUM OUTPUT AMPLITUDES AND ATTENUATION VALUES FOR STRUCTURE 2

s_{nv}, µm	V_{max}, mV	E_{att}, dB
2200	70	17.1
7700	75	16.5
13200	74	16.6

It is clear from it that V_{max} increases by 7% when s_{nv} increases from 2200 µm to 7700 µm, and decreases by 2% when s_{nv} increases from 7700 µm to 13200 µm. Then, s_{nv}=2200 µm is optimal for further field tests.

IV. FIELD TESTS AND ANALYSIS

A prototype of Structure 2 with s_{nv}=2200 µm was fabricated for field tests. This prototype is shown in Fig. 8 without RAM to demonstrate printed traces.

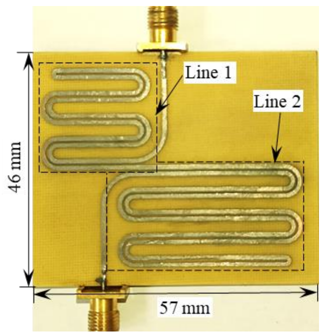

Fig. 8. Fabricated prototype without RAM

Its geometric parameters and substrate material are similar to the original. The size of the PCB with Structure 2 in Fig. 8 is 46 mm × 57 mm. The length of the first line is l_1=21 mm, and the length of the second line is l_2=36 mm. The difference between lines length of the model in Fig. 6 and the manufactured prototype can be explained by the presence of the interconnects, the length of which was not taken into account in the quasi-static simulation.

Experimental studies were performed by measuring S-parameters of the prototype and then using them to calculate the time response to a given excitation. They were measured for the prototype without and with RAM. Liquid RAM was added to fix the solid RAM to the prototype and to eliminate air gaps between the radio absorbing layer and the board. In addition, we performed electrodynamic simulation to validate the results.

S-parameters were measured using a Micran P4M-18 vector network analyzer with an operating frequency range from 10 MHz to 20 GHz. The manufactured prototype was connected to its 2 ports via SMA connectors using high frequency cables. The measurement setup for analyzing the frequency characteristics is shown in Fig. 9.

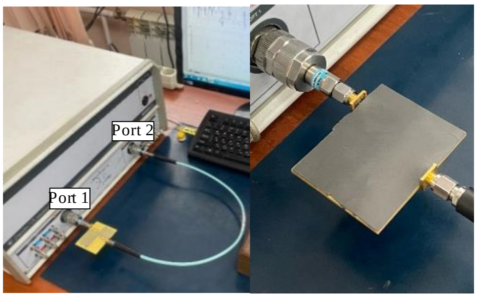

(a) (b)

Fig. 9. Setup for measuring Structure 2: (a) without RAM, (b) with RAM

Figure 10 shows the measured frequency dependence of $|S_{21}|$ of Structure 2 without and with RAM to demonstrate the bandwidth and attenuation of interference pulses up to 10 GHz.

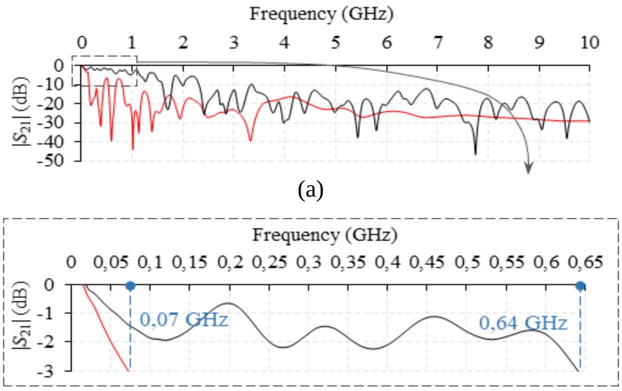

(b)

Fig. 10. Measured frequency dependencies of $|S_{21}|$ of Structure 2: (a) without RAM (—), (b) with RAM (—)

It is clear that when applying RAM to Structure 2 in the range up to 3.5 GHz, the attenuation increases (e.g., at 1 GHz up to -44 dB), and in the range from 2 GHz to 10 GHz, the number of resonances significantly decreases compared to Structure 2 without RAM. In addition, the cut-off frequency is also reduced. With RAM it is 0.07 GHz, and without RAM – 0.64 GHz.

Figure 11 shows the voltage waveforms at the output of Structure 2 without and with RAM calculated from its measured *S*-parameters and electrodynamic simulation.

Note that liquid RAM has properties different to solid RAM. Therefore, this was taken into account in the electrodynamic simulation – ε_{rr} and tgδ of the layer with RAM were assumed to be 8 and 0.1. Fig. 11 shows that simulation and experimental results are in good agreement. Table 2 summarizes the V_{max} and E_{att} for all cases considered in Fig. 11.

It is known that USPs are dangerous for electronic devices [7]. For example, its large amplitude can lead to electrical breakdown, fast rise time – to spark formation, average effective voltage value – to component burnout, etc. Therefore, we used *N*-norms [19, 20], which were used in similar studies [21], to evaluate the probability of these factors. The names, formulas and descriptions of each norm are known from [22, 23]. The *N*- norms calculated in the 50 Ω tract without line and in Structure 2 with and without RAM are given in Table 3.

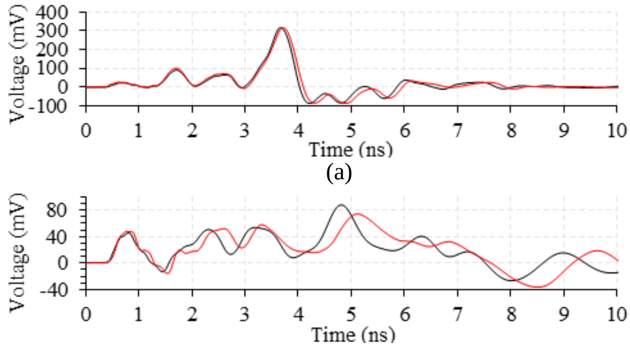

(b)

Fig. 11. Signal waveforms at the output of Structure 2 obtained by experiment (—) and by electrodynamic simulation (—): (a) without RAM, (b) with RAM

TABLE 2
THE MAXIMUM OUTPUT AMPLITUDES AND ATTENUATION VALUES

Case	*Without RAM*		*With RAM*	
	V_{max}, mV	E_{att}, dB	V_{max}, mV	E_{att}, dB
Electrodynamic simulation	318	3.94	70	16.7
Experiment	316	3.98	90	15.2

TABLE 3
MEASURED *N*-NORMS

Case	$N1\cdot10^{3}$	$N2\cdot10^{-9}$	$N3\cdot10^{10}$	$N4\cdot10^{10}$	$N5\cdot10^{6}$
Without line	500	2.5	2	2	9.13
At the line output with RAM	87	0.19	1.92	3.09	3.13
At the line output without RAM	316	1.29	1.98	3.94	6.89

It is clear from it that in Structure 2 with RAM, *N*1, *N*2, *N*3, and *N*5 decreased by 5.75 times, 13.16 times, 1.04 times, and 2.92 times, and *N*4 increased by 1.54 times. This reduced the probability of electrical breakdown, arc discharge, dielectric breakdown and component burnout. However, the probability of equipment damage caused by the total energy of the pulse was increased. Note that in Structure 2 without RAM the results were slightly worse: *N*1, *N*2, *N*3, and *N*5 decreased by 1.58 times, 1.94 times, 1.01 times, and 1.32 times, and *N*4 increased by 1.97 times. Thus, the use of Structure 2 with RAM for protection is more effective than without RAM.

This structure can be used in DC power circuits where phase distortion is acceptable. For example, according to the IPC-2221A standard [24], the line can be used in circuits with voltages and currents up to 530 V and 850 mA. It can also be used in circuits with higher voltages, but in that case additional optimization of its parameters is required (increase in minimum clearances and conductor area).

V. CONCLUSION

Practical realization of a two-turn meander MSL with reduced size has been performed. For this purpose, two approaches were applied: the use of RAM and additional folding of each ML turn into non-core turns. It was found that the sequence of arrival of decomposed pulses in the structure with RAM differs from the same structure without RAM. In this regard, new conditions of USP decomposition were formulated. It was also found that the folding of each turn of the meander MSL into non-core turns leads to additional USP attenuation. As a result of simulation, the USP attenuation was 16.3 dB. According to the experimental results, the USP attenuation was 15.3 dB. The size of the fabricated prototype was 46 mm × 57 mm, while without using RAM and folding, it is 10 mm × 575 mm. In addition, in such an unfolded structure without RAM, the USP attenuation is only 4.08 dB. The *N*-norm analysis of the structure showed that *N*1, *N*2, *N*3, and *N*5 decreased by 5.75 times, 13.16 times, 1.04 times, and 2.92 times, while *N*4 increased by 1.54 times. Thus, when using a manufactured prototype for USP protection, the probabilities of electrical breakdown, arc fault, dielectric breakdown, and component burnout can be reduced. However, the probability of equipment damage caused by the total pulse energy increases. Therefore, it is necessary to take this into account when using proposed structure in electronic devices where *N*4 is critical. The structure can be used in DC power supply circuits with voltages and currents up to 530 V and 850 mA.

ACKNOWLEDGEMENT

The research was supported by the Russian Science Foundation, Project 24-79-00102 (modeling) and the Ministry of Science and Higher Education of the Russian Federation, Project FEWM-2024-0005 (simulation) in TUSUR.

REFERENCES

[1] F. Sabath, “A Systematic Approach for Electromagnetic Interference Risk Management,” *IEEE Electromagnetic Compatibility Magazine*, vol. 6, no. 4, pp. 99–106, 2017, DOI: 10.1109/memc.0.8272296

[2] N. M. Parra, “Contribution to The Study of The Vulnerability of Critical Systems to Intentional Electromagnetic Interference (IEMI),” *Ph.D.dissertation*, Ecole Polytechnique Federale de Lausanne, 2016

[3] W. A. Radasky, "Fear of Frying Electromagnetic Weapons Threaten Our Data Networks. Here's How to Stop Them," *IEEE Spectrum*, vol. 51, no. 9, pp. 46-51, Sept. 2014, DOI: 10.1109/MSPEC.2014.6882988

[4] A. Nateghi, M. Schaarschmidt, S. Fisahn, and H. Garbe, “Susceptibility of Power Line Communication (PLC) Channel to DS, AM and Jamming Intentional Electromagnetic Interferences,” *2021 Asia-Pacific International Symposium on Electromagnetic Compatibility (APEMC)*, Sep. 2021, DOI: 10.1109/apemc49932.2021.9596789

[5] L. Devaraj, A. R. Ruddle, and A. P. Duffy, “Electromagnetic Risk Analysis for Emi Impact on Functional Safety with Probabilistic Graphical Models and Fuzzy Logic,” *IEEE Letters on Electromagnetic Compatibility Practice and Applications*, vol. 2, no. 4, pp. 96–100, Dec. 2020, DOI: 10.1109/lemcpa.2020.3017483

[6] B. D. Oakes, L.-G. Mattsson, P. Näsman, and A. A. Glazunov, “A Systems-Based Risk Assessment Framework For Intentional Electromagnetic Interference (IEMI) on Critical Infrastructures,” *Risk Analysis*, vol. 38, no. 6, pp. 1279–1305, Jan. 2018, DOI: 10.1111/risa.12945

[7] D. Tsyanenka, V. Mordachev, E. Sinkevich, A. Galenko, X. Ma, and W.-Q. Guo, “UWB EMP Susceptibility Testing of General-Purpose Electronic, Radio Communication, and Industrial Equipment,” *2021 Asia-Pacific International Symposium on Electromagnetic Compatibility (APEMC)*, Sep. 2021, DOI: 10.1109/apemc49932.2021.9597130

[8] Z.M. Gizatullin and R.M.Gizatullin, ”Investigation of The Immunity of Computer Equipment to The Power-Line Electromagnetic Interference,” *Journal of Communications Technology and Electronics*. Vol. 61. no. 5, pp. 546–550., 2016, DOI: 10.1134/S1064226916050053

[9] D. Packiaraj, K. J. Vinoy, M. Ramesh, and A. T. Kalghatgi, “Analysis of Multi-Conductor Coupled Microstrip Lines with An Aperture in The Ground Plane for The Design of a Broadband Filter,” *Journal of Electromagnetic Waves and Applications*, vol. 27, no. 7, pp. 856–867, Apr. 2013, DOI: 10.1080/09205071.2013.789410

[10] Y. He et al., "Common-Mode Filtering in Multilayer Printed Circuit Boards," *2017 IEEE International Symposium on Electromagnetic Compatibility & Signal/Power Integrity (EMCSI)*, Washington, DC, 2017, pp. 288-292, DOI: 10.1109/ISEMC.2017.8077882

[11] Q. Liu, S. Xu and D. Pommerenke, "PCB Structures for Common Mode Suppression on Differential Microstrip Lines," *2014 IEEE International Symposium on Electromagnetic Compatibility (EMC)*, Raleigh, NC, USA, 2014, pp. 533-537, DOI: 10.1109/ISEMC.2014.6899029

[12] R. S. Surovtsev, A. V. Nosov, A. M. Zabolotsky, and T. R. Gazizov, “Possibility of Protection Against UWB Pulses Based on A Turn of A Meander Microstrip Line,” *IEEE Transactions on Electromagnetic Compatibility*, vol. 59, no. 6, pp. 1864–1871, Dec. 2017, DOI: 10.1109/temc.2017.2678019

[13] A. V. Nosov, R. S. Surovtsev and T. R. Gazizov, "Propagation of UWB Pulse in Two Turns of Meander Microstrip Line Connected in Cascade," *2019 International Multi-Conference on Engineering, Computer and Information Sciences (SIBIRCON)*, Novosibirsk, Russia, 2019, pp. 0288-0292, DOI: 10.1109/SIBIRCON48586.2019.8958349

[14] G. Y. Kim, A. V. Nosov, R. S. Surovtsev, T. T. Gazizov, and A. E. Maximov, “Conditions for Ultrashort Pulse Decomposition in Multi-Cascade Protection Devices Based on Meander Microstrip Lines,” *Journal of Physics: Conference Series*, vol. 1679, no. 2, p. 022059, Nov. 2020, DOI: 10.1088/1742-6596/1679/2/022059

[15] Y. S. Zhechev, A. H. Adnan, and K. P. Malygin, “New Technique for Improving Modal Filter Performance by Using an Electromagnetic Absorber,” *IEEE Access*, vol. 10, pp. 86663–86670, 2022, DOI: 10.1109/access.2022.3199360

[16] K. P. Malygin and A. V. Nosov, "Experimental Confirmation of Ultrashort Pulse Decomposition in Folded Meander Microstrip Lines," *in IEEE Transactions on Electromagnetic Compatibility*, vol. 66, no. 2, pp. 599-605, April 2024, DOI: 10.1109/TEMC.2023.3328551

[17] S.P. Kuksenko, “Preliminary Results of TUSUR University Project for Design of Spacecraft Power Distribution Network: EMC Simulation,” *IOP Conference Series: Materials Science and Engineering*, vol. 560, pp. 1–7, 2019, DOI: 10.1088/1757-899X/560/1/012110

[18] G. Y. Kim, A. V. Nosov, and R. S. Surovtsev, “Improving the Analysis of the Propagation of Impulse Signals in Structures of N Cascades of Coupled Lines,” *Problems of Advanced Micro- and Nanoelectronic Systems Development*, pp. 82–88, 2022, DOI: 10.31114/2078-7707-2022-3-82-88

[19] C. E. Baum, “Norms and eigenvector norms.” *Mathematics Notes* 63, pp. 1–42, 1979.

[20] N. Mora, F. Vega, G. Lugrin, F. Rachidi and M. Rubinstein, *2014 System Design and Assessment Notes* 41

[21] Y. S. Zhechev, A. V. Zhecheva, A. A. Kvasnikov, and A. M. Zabolotsky, “Using *N*-norms for Analyzing Symmetric Protective Electrical Circuits with Triple Modal Reservation,” *Symmetry*, vol. 13, no. 12, p. 2390, 2021, DOI: 10.3390/sym13122390

[22] D. V. Giri, “High-Power Electromagnetic Radiators: Nonlethal Weapons and Other Applications.” *Harvard University Press*, Cambridge, MA, 2004

[23] IEC 61000–4–33. “Electromagnetic Compatibility (EMC) – Part 4–33: Testing and Measurement Techniques - Measurement Methods for High-Power Transient Parameters.” *Ed: IEC*, 2005

[24] IPC-2221A. “Generic Standard on Printed Board Design”, *Ed: IPC*, 2003